

Article

Effective Similarity Variables for the Computations of MHD Flow of Williamson Nanofluid over a Non-Linear Stretching Surface

Kamran Ahmed ¹, Luthais B. McCash ², Tanvir Akbar ¹ and Sohail Nadeem ^{3,*}

¹ Department of Mathematics, Islamabad Campus, COMSATS University Islamabad, Park Road, Islamabad 45550, Pakistan; kam_ahm@ymail.com (K.A.); tanvir.akbar@comsats.edu.pk (T.A.)

² School of Mathematics & Actuarial Science, University of Leicester, Leicester LE1 7RH, UK; lmccash@fb-fa.com

³ Department of Mathematics, Quaid-i-Azam University, Islamabad 44000, Pakistan

* Correspondence: sohail@qau.edu.pk

Abstract: The present study concerns investigating the two-dimensional Magnetohydrodynamics (MHD) boundary layer flow of Williamson nanofluid over a non-linear stretching sheet. The focus of this study is based on the global influence of the non-Newtonian Williamson fluid parameter (λ) rather than the local one that exists in the literature for linear and non-linear stretching cases. The mathematical model of the problem is based on the law of conservation of mass, momentum, and energy. The derived partial differential equations are transformed into ordinary differential equations by applying an appropriate similarity transformation. The subsequent equations are solved numerically by using the Shooting method. The physical quantities Skin friction coefficient, as well as the Sherwood and Nusselt numbers are computed locally. To validate the implemented shooting method, a comparison is made with the results obtained by Matlab function `bvp4c`, and good agreement is found. The Prandtl number, Pr , has an increasing impact of 25.14% on the wall temperature gradient. The impact of various physical parameters are presented through graphs and tables.

Keywords: similarity transformation; non-linear stretching sheet; Williamson nanofluid; shooting method; `bvp4c`



Citation: Ahmed, K.; McCash, L.B.; Akbar, T.; Nadeem, S. Effective Similarity Variables for the Computations of MHD Flow of Williamson Nanofluid over a Non-Linear Stretching Surface. *Processes* **2021**, *10*, 1119. <https://doi.org/10.3390/pr10061119>

Academic Editors: Byeong-Ui Moon and Tae-Hyeong Kim

Received: 19 May 2021

Accepted: 3 July 2021

Published: 2 June 2022

Publisher's Note: MDPI stays neutral with regard to jurisdictional claims in published maps and institutional affiliations.



Copyright: © 2021 by the authors. Licensee MDPI, Basel, Switzerland. This article is an open access article distributed under the terms and conditions of the Creative Commons Attribution (CC BY) license (<https://creativecommons.org/licenses/by/4.0/>).

1. Introduction

The two main categories of fluid mechanics are Newtonian and non-Newtonian fluid. The relationship among strain rate is described by deriving the constitutive equation, especially for those fluids that do not maintain the Newtonian law of viscosity. Several researchers have provided mathematical models to determine the rheological properties of such fluids. The models include the power-law, Williamson fluid, Ellis, cross, and Carreau models. Williamson [1] provided the Williamson model for pseudoplastic materials, which is an experimentally verified model. The characteristic of the Williamson fluid model involves choosing minimum (μ_0) and maximum (μ_∞) viscosity at the same time. In real fluid, minimum as well as maximum viscosity is needed for the mathematical model. Pseudoplastic fluids are commonly used in industry as melts of high molecular weight polymer solution, photographic film, and extrusion of polymer sheets [2]. Carmer et al. [3] investigated polymer solution using the Williamson fluid model. Lyubimov and Perminov [4] deliberated the flow of Williamson fluid over an inclined wall, with aspects of the gravitational field. Nadeem et al. [5] investigated the numerical solution of the peristaltic flow of Williamson fluid by radially varying MHD in an endoscope. Noreen Sher Akbar et al. [6] used the Carreau model and Ismail et al. [7] used the power-law model to investigate flow of blood in arteries. Ahmed et al. [8] numerically scrutinized the impact of Williamson fluid flow over an exponential stretching surface. Ramzan et al. [9]

performed linear analysis of heat transfer in three-dimensional Williamson nanofluid with a Cattaneo-Christov heat flux model.

In the industrial process, liquids' thermal features play an essential role in requirements such as in heating and cooling [10–13]. The transfer of heat performance of a liquid is regulated by its thermal conductivity. Furthermore, fluids' thermal conductivity via water, engine oil, and ethylene glycol is inherently low compared to that of solids [14,15]. Researchers have tried to escalate the thermal conductivity of such conventional heat transfer fluids using tiny particles of solids with high thermal conductivity. Many researchers have investigated the millimeter and micrometer dimensions of these solid suspensions, and significant drawbacks such as low thermal conductivity, particle sedimentation, excessive pressure drops, particle clogging, etc., were observed. By downsizing the particle size, the performance of heat transfer is improved in liquids [16–21]. With nanotechnology advancements, scientists on an atomic or molecular scale prepared a nanometer-sized particle with enhanced thermo-physical properties [22–26]. In a base fluid, the suspension of nanoparticles is known as nanofluid. It has been experimentally proven the nanofluid's thermal conductivity is higher than for base fluids. Inside the base fluid, the nanoparticles easily fluidize, due to which sedimentation and clogging of channels are no longer problems.

The heat transfer and the boundary layer flow over a stretching sheet are essential in engineering and industries due to their many applications [27–34]. At the final stage of processing, the final products' characteristics are highly dependent upon stretching and heat transfer rate. Under several stretching velocities, different natural processes take place. Such flow situations are encountered in numerous manufacturing processes, like polymer sheet production, extrusion from dye metal spinning, rubber sheet production, glass blowing, paper product manufacturing, annealing of copper wires and glass fiber, etc. Sakiadis [35–37] discussed the impact of constant velocity on Newtonian fluid due to a moving plate. The two-dimensional steady flow over a stretching linear surface was established for the first time by Crane [38]. Numerous authors further extended Crane's work by considering several physical phenomena, like the influence of the magnetic field, injection or suction, and heat transfer effects on such flow caused by a stretched surface. Gupta [39] investigated the stretching flow along with suction/injection. The influence of linear velocity on stretching/shrinking walls and consideration of hydromagnetic, chemical reaction, and viscous dissipation have been studied by Kameswaran [40]. Khan et al. [41] used an optimal homotopy analysis method to investigate heat transfer in a boundary layer nanofluid equipped with a Cattaneo-Christov heat flux model over an exponentially stretching surface.

MHD flows have fundamental importance from a scientific and applied point of view. The study involves the consideration of an applied magnetic field on the flow of electrically conducting fluid. The subject has developed to such an extent that it is not possible to refer to even a fraction of the literature and its applications. However, recognizing its importance, we will introduce MHD effects in the stretching phenomenon for non-Newtonian Williamson fluid. Some relevant background literature of interest will help to understand its significance for our purposes. The study of MHD flows induct theoretical and experimental work, which Hartmann and Lazarus performed. MHD has many applications in fields such as fusion reactors (blanket, diverter, limiter, F.W.), astrophysics (planetary magnetic field), crystal growth, ship propulsion, dispersion (granulation) of metals, jet printers, MHD pumps (1907), MHD flow meters (1935), MHD generators (1923), metallurgy (induction furnace as well as the casting of Al and Fe), magnetic filtration and separation, and MHD flow control (reducing turbulent drag) [42–46]. Hussain et al. [47] used the Keller box method to investigate the MHD convective flow of Williamson fluid with homogeneous-heterogeneous reactions.

The present paper aims to examine the influence of MHD Williamson nanofluid flow over a non-linear stretching sheet. The focus of this study is based on the global influence of the Non-Newtonian Williamson fluid parameter rather than the local one. To the best of

the authors' knowledge, the proposed model on similarity transformation has not yet been considered. The governing non-linear PDEs are reduced into the system of non-linear ODEs with the help of similarity transformation. The transformed equations are numerically solved by applying the shooting method and bvp4c. The dimensionless skin friction, wall temperature gradient, and Sherwood number are obtained and are displayed in Tables 1–3. The influence of the magnetic parameter, Prandtl number, diffusivity parameter, Williamson fluid parameter, Schmidt number, Lewis number, and heat capacity ratio on velocity, temperature, and concentration profiles are shown through graphs.

Table 1. Effect of physical parameters on the skin friction coefficient.

$\lambda \downarrow$	$M \uparrow$	Pr	Nbt	Nc	Le	Sc	$-(f''(0) + \frac{\lambda}{6} f''^2(0))$	
							Shooting Method	bvp4c
0.1	0.5	0.5	2.0	0.5	3.0	2.0	0.786446	0.786446
0.2	0.5	0.5	2.0	0.5	3.0	2.0	0.782473	0.782473
0.3	0.5	0.5	2.0	0.5	3.0	2.0	0.778424	0.778424
0.5	0.1	0.5	2.0	0.5	3.0	2.0	0.694890	0.694890
0.5	0.2	0.5	2.0	0.5	3.0	2.0	0.716547	0.716547
0.5	0.3	0.5	2.0	0.5	3.0	2.0	0.737670	0.737670

Table 2. Effect of physical parameters on Nusselt number $-\theta'(0)$.

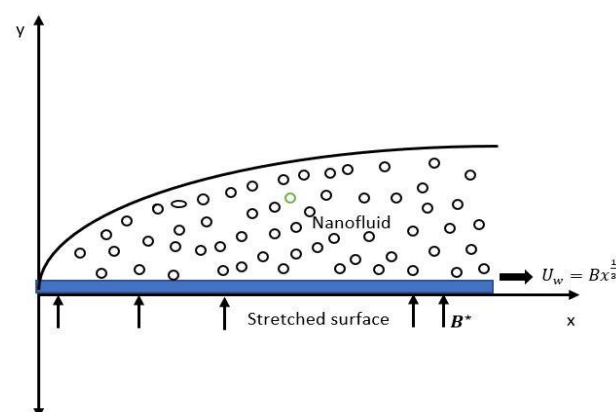
$\lambda \downarrow$	$M \downarrow$	$Pr \uparrow$	$Nbt \uparrow$	$Nc \downarrow$	$Le \uparrow$	Sc	$-\theta'(0)$	
							Shooting Method	bvp4c
0.1	0.5	0.5	2.0	0.5	3.0	2.0	0.288735	0.288735
0.2	0.5	0.5	2.0	0.5	3.0	2.0	0.288369	0.288369
0.3	0.5	0.5	2.0	0.5	3.0	2.0	0.287995	0.287995
0.5	0.1	0.5	2.0	0.5	3.0	2.0	0.294560	0.294560
0.5	0.2	0.5	2.0	0.5	3.0	2.0	0.292823	0.292823
0.5	0.3	0.5	2.0	0.5	3.0	2.0	0.291151	0.291151
0.5	0.5	0.1	2.0	0.5	3.0	2.0	0.189510	0.189510
0.5	0.5	0.2	2.0	0.5	3.0	2.0	0.212828	0.212828
0.5	0.5	0.3	2.0	0.5	3.0	2.0	0.237148	0.237148
0.5	0.5	0.5	0.4	0.5	3.0	2.0	0.249286	0.249286
0.5	0.5	0.5	0.5	0.5	3.0	2.0	0.258448	0.258448
0.5	0.5	0.5	0.6	0.5	3.0	2.0	0.264741	0.264740
0.5	0.5	0.5	2.0	0.1	3.0	2.0	0.326417	0.326417
0.5	0.5	0.5	2.0	0.2	3.0	2.0	0.316415	0.316415
0.5	0.5	0.5	2.0	0.3	3.0	2.0	0.306681	0.306681
0.5	0.5	0.5	2.0	0.5	0.3	2.0	0.062628	0.062628
0.5	0.5	0.5	2.0	0.5	0.4	2.0	0.097528	0.097528
0.5	0.5	0.5	2.0	0.5	0.5	2.0	0.126389	0.126389
0.5	0.5	0.5	2.0	0.5	3.0	0.1	0.304255	0.304254
0.5	0.5	0.5	2.0	0.5	3.0	0.2	0.302944	0.302944
0.5	0.5	0.5	2.0	0.5	3.0	0.3	0.301662	0.301662

Table 3. Effect of physical parameters on Sherwood number $-g'(0)$.

$\lambda \downarrow$	$M \downarrow$	$Pr \downarrow$	$Nbt \uparrow$	$Nc \uparrow$	$Le \downarrow$	$Sc \uparrow$	$-g'(0)$	
							Shooting Method	bvp4c
0.1	0.5	0.5	2.0	0.5	3.0	2.0	0.693244	0.693243
0.2	0.5	0.5	2.0	0.5	3.0	2.0	0.692233	0.692232
0.3	0.5	0.5	2.0	0.5	3.0	2.0	0.691192	0.691191
0.5	0.1	0.5	2.0	0.5	3.0	2.0	0.707605	0.707604
0.5	0.2	0.5	2.0	0.5	3.0	2.0	0.703351	0.703351
0.5	0.3	0.5	2.0	0.5	3.0	2.0	0.699200	0.699200
0.5	0.5	0.1	2.0	0.5	3.0	2.0	0.739933	0.739933
0.5	0.5	0.2	2.0	0.5	3.0	2.0	0.727616	0.727615
0.5	0.5	0.3	2.0	0.5	3.0	2.0	0.715347	0.715346
0.5	0.5	0.5	0.4	0.5	3.0	2.0	0.591692	0.591691
0.5	0.5	0.5	0.5	0.5	3.0	2.0	0.604384	0.604383
0.5	0.5	0.5	0.6	0.5	3.0	2.0	0.617227	0.617226
0.5	0.5	0.5	2.0	0.1	3.0	2.0	0.675000	0.675000
0.5	0.5	0.5	2.0	0.2	3.0	2.0	0.679217	0.679216
0.5	0.5	0.5	2.0	0.3	3.0	2.0	0.683319	0.683318
0.5	0.5	0.5	2.0	0.5	0.3	2.0	0.788938	0.788937
0.5	0.5	0.5	2.0	0.5	0.4	2.0	0.772636	0.772635
0.5	0.5	0.5	2.0	0.5	0.5	2.0	0.759863	0.759862
0.5	0.5	0.5	2.0	0.5	3.0	0.1	0.172203	0.172204
0.5	0.5	0.5	2.0	0.5	3.0	0.2	0.198512	0.198513
0.5	0.5	0.5	2.0	0.5	3.0	0.3	0.225899	0.225899

2. Problem Description

We considered the MHD two-dimensional steady boundary layer flow of an incompressible Williamson nanofluid over a non-linear stretching plate. We assumed that the plate is stretching along the x -axis, with the varying velocity $u = U_w = Bx^{\frac{1}{2}}$, and the y direction is taken perpendicular to the x direction, as shown in the Figure 1. The transverse magnetic field $B^* = \frac{B_0}{x^{\frac{1}{2}}}$ is exposed in a direction vertical to the flow. It is also supposed that U_w , T_w , and C_w are the velocity, temperature, and concentration profiles of the fluid at the surface, respectively. Moreover, the ambient temperature and concentration are taken to be T_∞ and C_∞ , respectively. The continuity, momentum, energy, and concentration equations are taken as specified by Nadeem and Hussain [48,49].

**Figure 1.** Flow geometry of the problem.

Cauchy stress tensor is defined as

$$S = -pI + \tau, \quad (1)$$

$$\boldsymbol{\tau} = \left[\mu_{\infty} + \frac{\mu_0 - \mu_{\infty}}{1 - \Gamma \dot{\gamma}} \right] \mathbf{A}_1, \quad (2)$$

where $\boldsymbol{\tau}$ represents the extra stress tensor, μ_{∞} and μ_0 are limiting viscosities at infinite and zero shear stress rates, respectively, \mathbf{A}_1 is the first Rivlin Ericksen tensor, $\Gamma > 0$ is the time constant, and $\dot{\gamma}$ is denoted as

$$\dot{\gamma} = \sqrt{\frac{1}{2} \pi}, \quad (3)$$

$$\pi = \text{trace}(\mathbf{A}_1)^2,$$

We choose the case in which $\mu_{\infty} = 0$ and $\Gamma \dot{\gamma} < 1$. Thus, Equation (2) takes the form

$$\boldsymbol{\tau} = \left[\frac{\mu_0}{1 - \Gamma \dot{\gamma}} \right] \mathbf{A}_1, \quad (4)$$

Applying Binomial expansion, we obtain

$$\boldsymbol{\tau} = \mu_0 [1 + \Gamma \dot{\gamma}] \mathbf{A}_1. \quad (5)$$

Under given conditions, the boundary layer momentum, energy, and concentration equation with the magnetic field are

$$\frac{\partial u}{\partial x} + \frac{\partial v}{\partial y} = 0, \quad (6)$$

$$u \frac{\partial u}{\partial x} + v \frac{\partial u}{\partial y} = \nu \frac{\partial^2 u}{\partial y^2} + \sqrt{2} \Gamma \nu \frac{\partial u}{\partial y} \frac{\partial^2 u}{\partial y^2} - \sigma \frac{B^*2}{\rho} u, \quad (7)$$

$$u \frac{\partial T}{\partial x} + v \frac{\partial T}{\partial y} = \alpha \frac{\partial^2 T}{\partial y^2} + \frac{\rho_p c_p}{\rho c} \left[D_B \frac{\partial C}{\partial y} \frac{\partial T}{\partial y} + \frac{D_T}{T_{\infty}} \left(\frac{\partial T}{\partial y} \right)^2 \right], \quad (8)$$

$$u \frac{\partial C}{\partial x} + v \frac{\partial C}{\partial y} = \frac{D_T}{T_{\infty}} \frac{\partial^2 T}{\partial y^2} + D_B \frac{\partial^2 C}{\partial y^2}, \quad (9)$$

The accompanying boundary conditions are

$$\begin{aligned} u &= U_w = Bx^{\frac{1}{3}}, \quad v = 0, \quad T = T_w, \\ C &= C_w, \quad \text{at } y = 0, \\ u &\rightarrow 0, \quad T \rightarrow 0, \quad C \rightarrow 0, \quad \text{as } y \rightarrow \infty. \end{aligned} \quad (10)$$

The following transformations are introduced:

$$\begin{aligned} \eta &= \frac{1}{x^{\frac{1}{3}}} \sqrt{\frac{B}{\nu}} y, \quad u = Bx^{\frac{1}{3}} f'(\eta), \\ v &= -\frac{\sqrt{\nu B}}{3x^{\frac{1}{3}}} (2f(\eta) - \eta f'(\eta)), \\ g &= \frac{C - C_{\infty}}{C_w - C_{\infty}}, \quad \theta = \frac{T - T_{\infty}}{T_w - T_{\infty}}. \end{aligned} \quad (11)$$

Using Equation (11) in Equations (6)–(10), Equation (6) is identically satisfied and Equations (7)–(10) take the following form:

$$\begin{aligned} 3f''' + 2ff'' + \lambda f'' f''' - Mf' - f'^2 &= 0, \\ \theta'' + \frac{2}{3} \text{Pr} f \theta' + \frac{Nc}{Le} g' \theta' + \frac{Nc}{Le \times Nbt} \theta'^2 &= 0, \\ g'' + \frac{2}{3} Sc f g' + \frac{1}{Nbt} \theta'' &= 0, \end{aligned} \quad (12)$$

$$\begin{aligned} f = 0, f' = 1, \theta = 1, g = 1, \text{ at } \eta = 0, \\ f' \rightarrow 0, \theta \rightarrow 0, g \rightarrow 0, \text{ as } \eta \rightarrow \infty. \end{aligned} \quad (13)$$

where $M = \frac{3\sigma B_0^2}{B\rho}$ represents a magnetic parameter, $\lambda = 3\Gamma\sqrt{\frac{2B^3}{\nu}}$ represents the Williamson parameter, $Nbt = \frac{D_B T_\infty (C_w - C_\infty)}{D_T (T_w - T_\infty)}$ is the diffusivity parameter, $Sc = \frac{\nu}{D_B}$ is the Schmidt number, $Pr = \frac{\nu}{\alpha}$ represents the Prandtl number, $Le = \frac{\alpha}{D_B}$ represents the Lewis number, and the heat capacity ratio is represented by $Nc = \frac{\rho_p c_p}{\rho c} (C_w - C_\infty)$.

The classical boundary layer equation for the viscous flow can be obtained from Equation (12) for $\lambda = M = 0$. That is, the fluid behaves as a Newtonian one.

2.1. Friction and Heat Transport Quantities

Some other physical quantities of concern in the current investigation are defined as

$$C_f = \frac{\tau_w}{\rho U_w^2}, Nu_x = \frac{xq_n}{T_w - T_\infty}, Sh_x = \frac{xq_s}{C_w - C_\infty}. \quad (14)$$

where C_f represents the local skin friction, Nu_x represents the local Nusselt number, and Sh_x represents the local Sherwood number. Shear stress at the wall τ_w , wall heat flux q_n , and wall mass flux q_s are defined as

$$\begin{aligned} \tau_w &= \left(\mu_o \left(\frac{\partial u}{\partial y} + \frac{\Gamma}{\sqrt{2}} \left(\frac{\partial u}{\partial y} \right)^2 \right) \right)_{y=0}, \\ q_n &= - \left(\frac{\partial T}{\partial y} \right)_{y=0}, q_s = - \left(\frac{\partial C}{\partial y} \right)_{y=0}. \end{aligned} \quad (15)$$

By using Equation (11) in Equation (15) and Equation (14), we obtain the dimensionless form

$$\begin{aligned} Re_x C_f &= \left(f'' + \frac{\lambda}{6} f''^2 \right)_{\eta=0}, \\ \frac{Nu_x}{Re_x} &= -\theta'(0), \frac{Sh_x}{Re_x} = -g'(0). \end{aligned} \quad (16)$$

where $Re_x = \sqrt{\frac{x^{\frac{2}{3}}}{B\nu}} U_w$ represents the local Reynolds number.

2.2. Solution Procedure

Non-linear ordinary differential Equation (12) is solved by applying the boundary conditions of Equation (13), in which the velocity profile involves third order, and temperature and concentration profiles are of second order. To solve non-linear ODEs, we use the Shooting method and `bvp4c` code. Equation (12) is transformed into the system of seven first-order ordinary differential equations. We use the following substitution:

$$f = \zeta_1, f' = \zeta_2, f'' = \zeta_3, \theta = \zeta_4, \theta' = \zeta_5, g = \zeta_6, g' = \zeta_7.$$

The derived system of simultaneous first-order differential equations is

$$\begin{aligned} \zeta_1' &= \zeta_2, \zeta_2' = \zeta_3, \zeta_3' = \frac{1}{3 + \lambda\zeta_3} (\zeta_2^2 - 2\zeta_1\zeta_3 + M\zeta_2) \\ \zeta_4' &= \zeta_5, \zeta_5' = -\frac{2}{3}Pr\zeta_1\zeta_5 - \frac{Nc}{Le}\zeta_7\zeta_5 - \frac{Nc}{Le \times Nbt}\zeta_5^2, \\ \zeta_6' &= \zeta_7, \zeta_7' = -\frac{2}{3}Sc\zeta_1\zeta_7 - \frac{1}{Nbt}\zeta_5'. \end{aligned} \quad (17)$$

The converted boundary conditions are

$$\begin{aligned}\zeta_1(0) &= 0, \zeta_2(0) = 1, \\ \zeta_3(0) &= a, \zeta_4(0) = 1, \\ \zeta_6(0) &= 1, \zeta_5(0) = b, \zeta_7(0) = c.\end{aligned}\tag{18}$$

To solve the above BVP (Equation (17)) subject to the boundary conditions (Equation (18)), we utilize the shooting technique together with the RK-Fehlberg method. To this end, we guess the three anonymous conditions are $\zeta_3(0) = a$, $\zeta_5(0) = b$, and $\zeta_7(0) = c$. The reasonable guesses for a , b , and c are chosen such that the corresponding known boundary conditions are almost satisfied for $\eta \rightarrow \infty$. Newton's iterative structure is applied to refine the initial guesses for a , b , and c until the preferred approximation is met. The stopping criteria for the iterative process are

$$\max(|\zeta_2(\eta_{max}) - 0|, |\zeta_4(\eta_{max}) - 0|, |\zeta_6(\eta_{max}) - 0|) < \varepsilon$$

where ε is a small positive real number. The computations in the rest of this article are performed with $\varepsilon = 10^{-6}$. The effect of various emerging parameters was investigated over an applicable bounded domain $[0, \eta_{max}]$ as a replacement for $[0, \infty)$. It is observed that for growing values of η_{max} , no substantial variations are detected in the results. In order to test the reliability of the implemented shooting method, the in-house built code was validated with MATLAB built-in `bvp4c` function.

3. Results and Discussion

The governing non-linear PDE Equations (6)–(9), along with boundary conditions (Equation (10)) of magnetohydrodynamic Williamson nanofluid over a non-linear stretching surface is converted into ODEs by applying the appropriate similarity transformation given by Equation (11). The resulting ODEs are numerically solved by applying the Shooting method and Matlab function `bvp4c`. The impact of involving parameters such as Magnetic parameter M , Williamson fluid parameter λ , Diffusivity parameter Nbt , Schmidt number Sc , Prandtl number Pr , Lewis number Le , heat capacity ratio Nc on velocity, and temperature and concentration profiles is depicted through graphs and tables. Table 1 illustrates the impact of λ and M on the skin friction coefficient. It shows that as we increase the Williamson fluid parameter λ , the value of the skin friction decreases. This is because the higher the Williamson parameter, the smaller the viscosity, which results in a skin friction coefficient reduction. By raising the value of the magnetic field parameter M , the value of the skin friction increases. The reason is that the magnetic field reduces fluid velocity, and as a consequence, the value of the skin friction increases.

Table 2 presents the effects of λ , M , Pr , Nbt , Nc , Le , and Sc on $-\theta'(0)$. By increasing the value of λ , the value for $-\theta'(0)$ declines, because the collision of the fluid particle slows down. Moreover, the higher the values of the magnetic field parameter M , the lesser is the wall temperature gradient. When we increase Pr , which describes correlation between kinematic viscosity and thermal diffusivity, the Nusselt number $-\theta'(0)$ increases; that is, the temperature gradient at the surface is increased. By increasing the value of the diffusivity ratio (Nbt), the value of the $-\theta'(0)$ increases because Nbt is the ratio of Brownian diffusivity to thermophoretic diffusivity, and Nbt increases because Brownian diffusivity increases, while it drops down on raising the heat capacities ratio, Nc . The Lewis number Le has an increasing effect on $-\theta'(0)$. By augmenting the value of Le , the thermal diffusivity is increased, resulting in growth in $-\theta'(0)$.

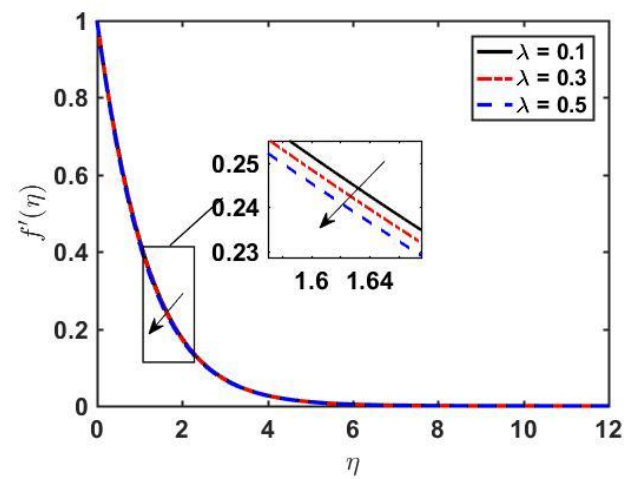
Table 3 presents the effects of λ , M , Pr , Nbt , Nc , Le , and Sc on $-g'(0)$. By enhancing the value of the Williamson fluid parameter λ , $-g'(0)$ decreases because of a decrease in resistance at the wall. Similar behavior of $-g'(0)$ is noted upon augmenting the values of magnetic parameter M and the Prandtl number Pr . With the increase in diffusivity ratio Nbt , the Sherwood number, $-g'(0)$, increases. This is because of the greater Brownian motion of fluid particles. When increasing the heat capacities ratio Nc , an increasing trend is seen for $-g'(0)$. Since Nc is the ratio of the heat capacities of nanoparticles to nanofluid,

enhancing N_c values mean an increase in nanoparticle heat capacity. It is discerned that the greater the Lewis number Le , the smaller the $-g'(0)$. When increasing the value of the Schmidt number Sc , the value of the $-g'(0)$ also increases. A comparison of Nusselt numbers from the present study and those from Nadeem et al. [48] for different values of Prandtl and Williamson fluid parameters between nonlinear and linear stretching is given in Table 4. It is readily seen that for both the parameters, the Nusselt number behavior is similar for both linear and nonlinear stretching cases, but its value is higher in the case of nonlinear stretching.

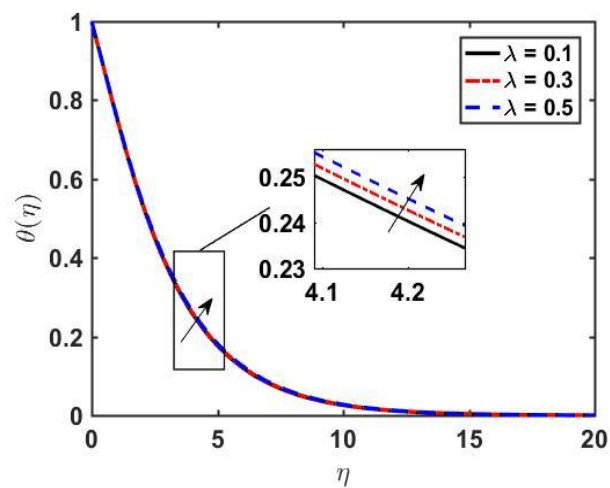
Table 4. Comparison between linear and nonlinear stretching for $-\theta'(0)$ by fixing $Le = 4$, $M = 0$, $N_{bt} = 2$, $N_c = 0.5$, $Pr = 0.5$, and $Sc = 0.5$.

λ	Pr	Linear Stretching—Nadeem et al. [48]	Nonlinear Stretching—Present Study
0.0		0.314	0.319
0.2		0.309	0.318
0.4		0.302	0.317
	0.2	0.144	0.231
	0.6	0.355	0.347
	1.2	0.588	0.521

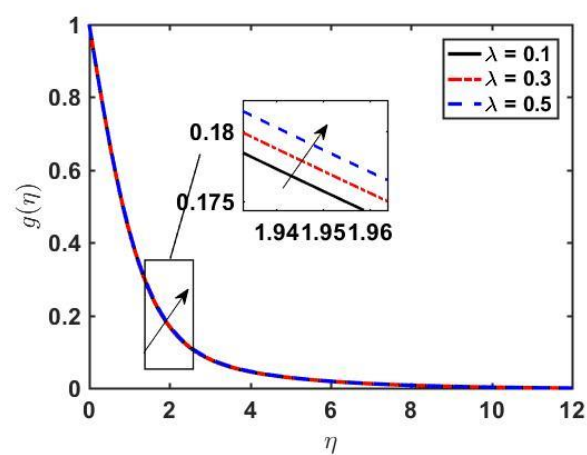
Figure 2 illustrates the impact of λ on $f'(\eta)$, $\theta(\eta)$, and $g(\eta)$. We observe that $f'(\eta)$ decreases as we increase λ . Physically, we can conclude that λ offers more resistance to velocity (see Figure 2a). Increasing of λ implies Γ retardation time is higher, which is responsible for the fluid particles regaining their actual position. As a result, the viscosity becomes higher, and the values of temperature and concentration profiles go up. Figure 2b,c describe the influence of the Williamson fluid parameter λ on $\theta(\eta)$ and $g(\eta)$. By increasing the value of λ , both the temperature and concentration profiles increase because of an increase in the fluid's resistivity. Figure 3 displays the effect of magnetic parameter M on $f'(\eta)$, $\theta(\eta)$, and $g(\eta)$. As we increase M , the velocity of the fluid decreases, and both temperature and concentration profiles increase. The Lorentz force, which is an opposing force, slows down the motion of fluid, and the velocity boundary layer thickness diminishes. The outcomes of Prandtl Pr on temperature distribution and concentration profile are presented in Figure 4. As we increase the Prandtl number Pr , the temperature profile decreases, and a reduction in the thermal boundary layer is noticed. The increasing of the Prandtl number Pr means making the kinematic viscosity stronger than thermal diffusivity and, as a result, more resistant to fluid flow. The Prandtl number shows the dual behavior on the concentration profile; as we increase the Prandtl number Pr , initially the concentration increases, and at $\eta = 2$ it changes its behavior from increasing to decreasing. This is because, far from the surface, viscous forces have negligible effects. Figure 5a,b depicts the effect of the Lewis Number Le on $\theta(\eta)$ and $g(\eta)$. As Le is increased, the temperature profile $\theta(\eta)$ decreases and the thickness of the thermal boundary layer also decreases, and the opposite behavior of the concentration profile $g(\eta)$ is seen.



(a)

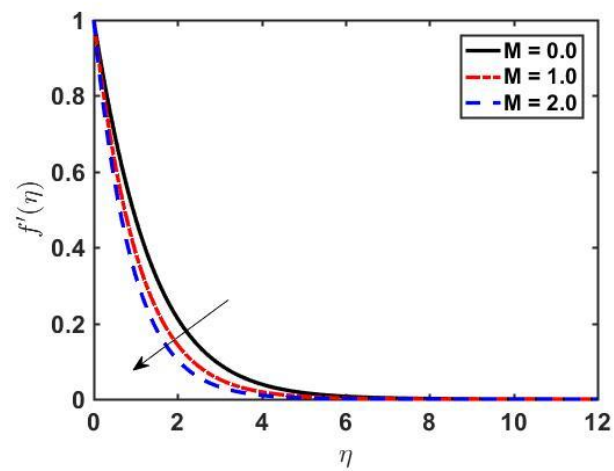


(b)

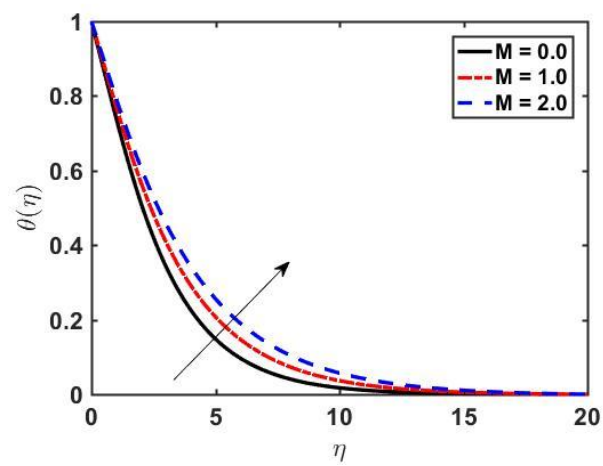


(c)

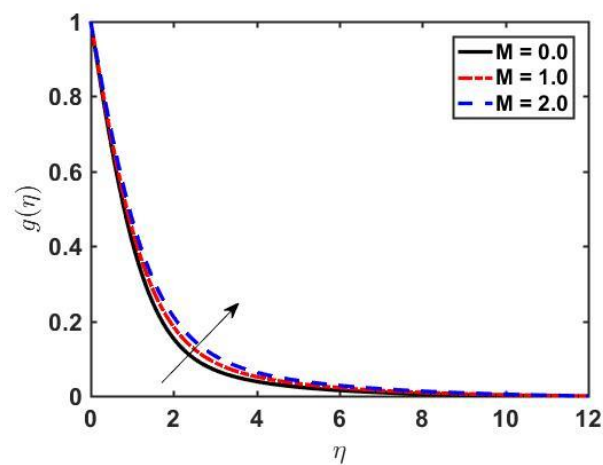
Figure 2. Profiles of $f'(\eta)$, $\theta(\eta)$, and $g(\eta)$ versus η for various values of λ by fixing $M = 0.5$, $Pr = 0.5$, $Le = 3.0$, $Nbt = 2.0$, $Nc = 0.5$, $Sc = 2.0$.



(a)



(b)



(c)

Figure 3. Profiles of $f(\eta)$, $\theta(\eta)$, and $g(\eta)$ versus η for various values of M , fixing $\lambda = 0.3$, $Pr = 0.5$, $Le = 3.0$, $Nbt = 2.0$, $Nc = 0.5$, and $Sc = 2.0$.

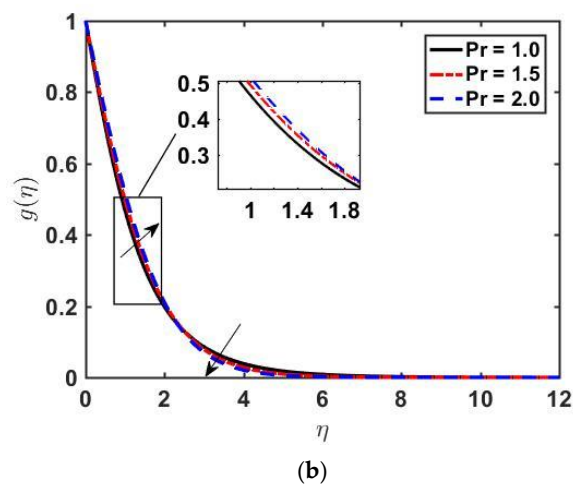
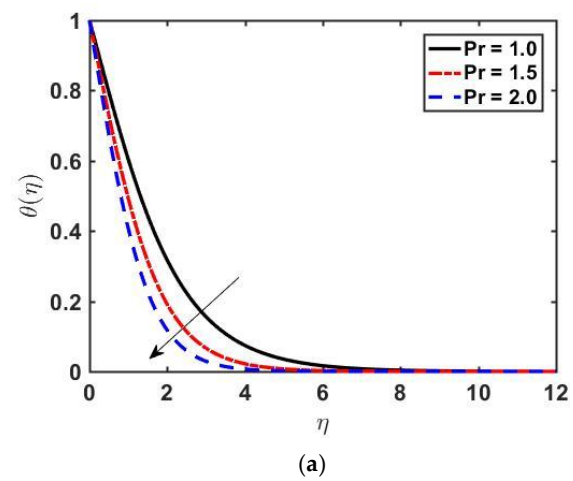


Figure 4. Profiles of $\theta(\eta)$ and $g(\eta)$ versus η for various values of Pr by fixing $\lambda = 0.3$, $M = 0.5$, $Le = 3.0$, $Nbt = 2.0$, $Nc = 0.5$, and $Sc = 2.0$.

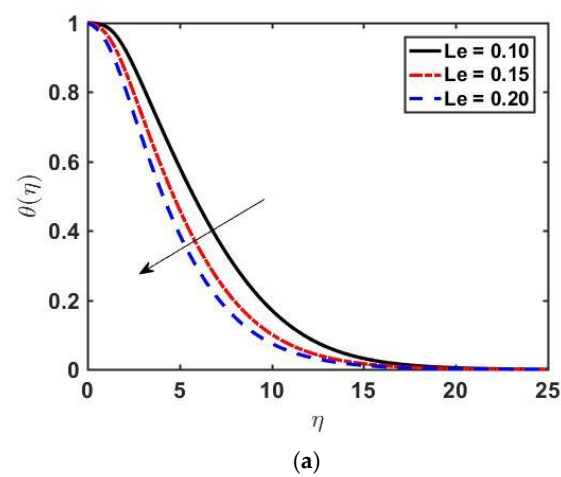


Figure 5. Cont.

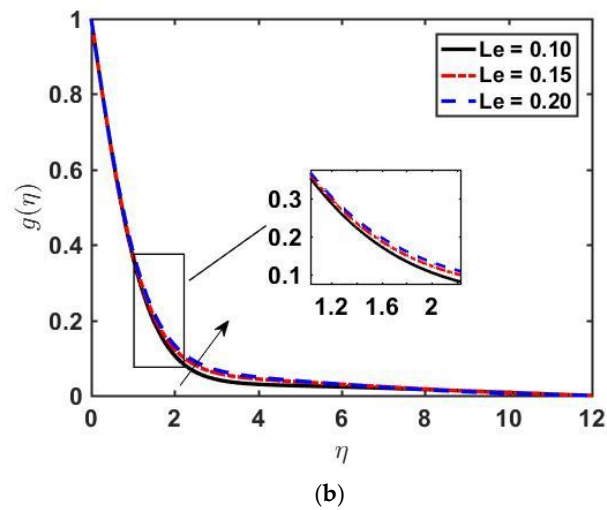


Figure 5. Profiles of $\theta(\eta)$ and $g(\eta)$ versus η for various values of Le by fixing $\lambda = 0.3$, $M = 0.5$, $Pr = 0.5$, $Nbt = 2.0$, $Nc = 0.5$, and $Sc = 2.0$.

For enormous values of t , the contribution of last terms of the second and third equations of Equation (12) is negligible; therefore, the concentration profile turns out to be free of temperature. The effect of diffusivity ratio Nbt on both $\theta(\eta)$ and $g(\eta)$ is manifested in Figure 6a,b. By increasing Nbt , both $\theta(\eta)$ and $g(\eta)$ decrease. The decrease in $g(\eta)$ is more rapid than $\theta(\eta)$, and a decrease in thermal boundary layer thickness is also witnessed. The influence of heat capacity ratio Nc on temperature and concentration profiles is shown in Figure 7a,b. The temperature profile $\theta(\eta)$ increases with an increase in Nc , while a depreciation in the concentration profile $g(\eta)$ is spotted. The effect of Sc on the concentration is shown in Figure 8. By raising the Schmidt number, the concentration profile is decreased. Since Sc is the ratio of momentum diffusivity and Brownian diffusivity, an increase in Sc results in a decreased Brownian diffusivity, which causes a weaker concentration profile.

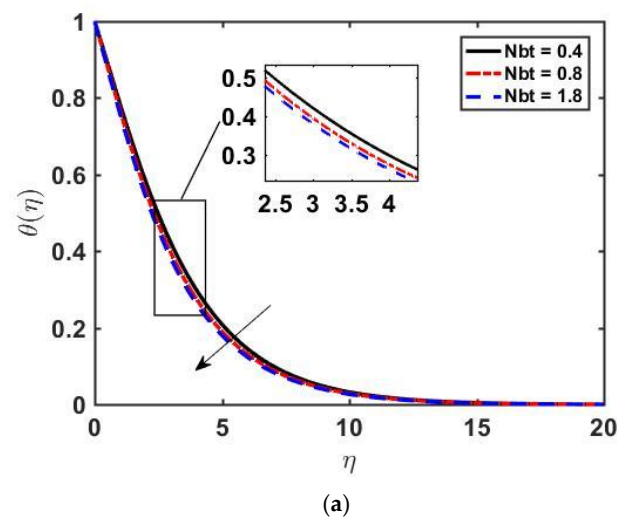


Figure 6. Cont.

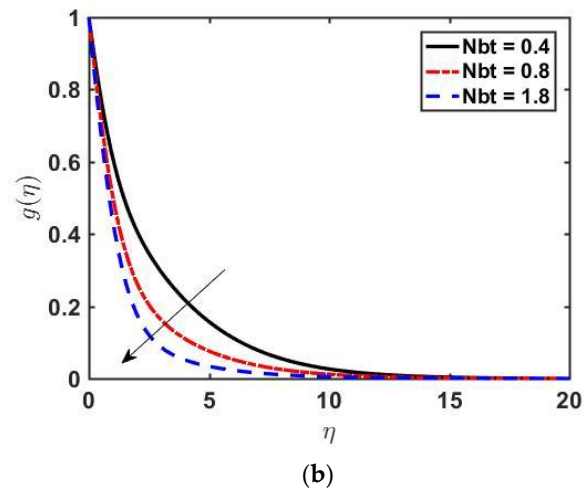


Figure 6. Profiles of $\theta(\eta)$ and $g(\eta)$ versus η for various values of Nbt by fixing $\lambda = 0.3$, $M = 0.5$, $Pr = 0.5$, $Le = 3.0$, $Nc = 0.5$, and $Sc = 2.0$.

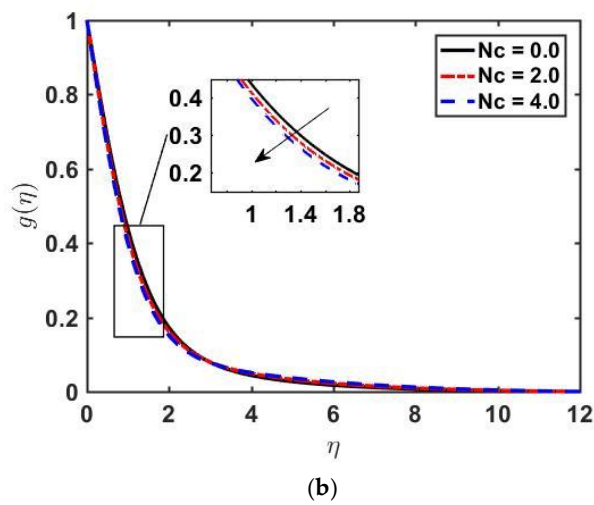
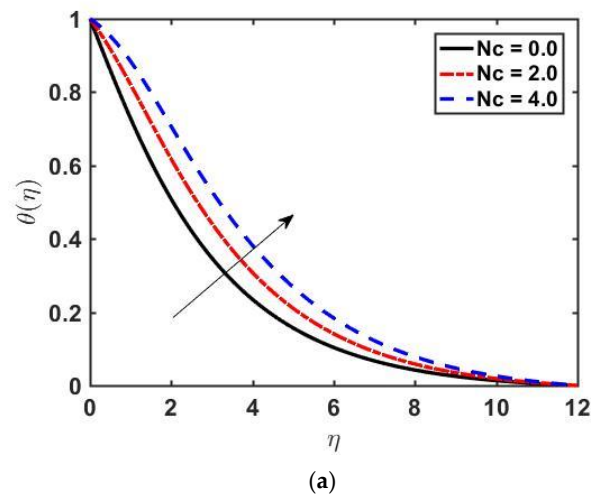


Figure 7. Profiles of $\theta(\eta)$ and $g(\eta)$ versus η for various values of Nc by fixing $\lambda = 0.3$, $M = 0.5$, $Pr = 0.5$, $Le = 3.0$, $Nbt = 2.0$, and $Sc = 2.0$.

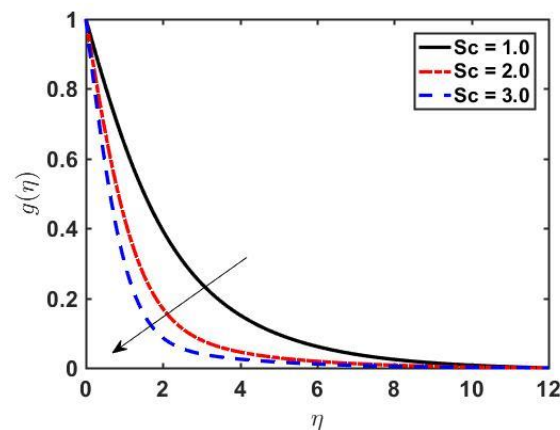


Figure 8. Profile of $g(\eta)$ versus η for various values of Sc by fixing $\lambda = 0.3$, $M = 0.5$, $Pr = 0.5$, $Le = 3.0$, $Nbt = 2.0$, and $Nc = 0.5$.

4. Conclusions

In this article, we modeled the MHD flow of Williamson nanofluid over a non-linear stretching surface. Similarity transformations were applied, and we obtained a system of non-linear ordinary differential equations. The shooting method was applied to solve them numerically. The combined effects of Williamson parameter λ , magnetic parameter M , diffusivity ratio Nbt , Prandtl number Pr , Lewis number Le , Schmidt number Sc , and heat capacities ratio Nc on heat and mass transfer of MHD boundary layer flow of Williamson nanofluid were examined. The salient features of this study are mentioned below:

- The Williamson parameter λ and magnetic parameter M have opposite impacts on skin friction coefficient.
- The wall temperature gradient decreases when increasing the value of Williamson parameter λ , magnetic parameter M , and heat capacities ratio Nc , whereas it increases for Prandtl number Pr , diffusivity ratio Nbt , and Lewis number Le . Moreover, the Lewis number Le reveals a strong effect on wall temperature gradient $-\theta'(0)$.
- The diffusivity ratio Nbt , heat capacities ratio Nc , and the Schmidt number Sc show direct relation with the Sherwood number $-g'(0)$. An opposite relation is seen with Williamson parameter λ , magnetic parameter M , Prandtl number Pr , and Lewis number Le . It is worth mentioning that the most substantial outcome is seen for the Schmidt number Sc , where there is a 31% increment in the Sherwood number.
- When raising the values of Williamson parameter λ and magnetic parameter M , the velocity profile settles at lower values, whereas the temperature and concentration profile settles at higher values. Moreover, the velocity boundary layer contracts, and the thermal boundary layer enlarges.
- The temperature profile settles at lower values when raising the Prandtl number Pr , Lewis number Le , and diffusivity ratio Nbt .
- The concentration profile shows direct relation to the Lewis number Le and an inverse relation to diffusivity Nbt , heat capacities ratio Nc , and Schmidt number Sc , whereas Prandtl number Pr shows dual behavior.

Author Contributions: Conceptualization, K.A. and T.A.; methodology, L.B.M.; software, S.N.; validation, K.A., T.A. and L.B.M.; formal analysis, S.N.; investigation, K.A.; resources, L.B.M.; data curation, T.A.; writing—original draft preparation, K.A.; writing—review and editing, S.N.; visualization, S.N.; supervision, T.A.; project administration, T.A.; funding acquisition, L.B.M. All authors have read and agreed to the published version of the manuscript.

Funding: This research received no external funding.

Institutional Review Board Statement: Not applicable.

Informed Consent Statement: Not applicable.

Data Availability Statement: Not applicable.

Conflicts of Interest: The authors declare no conflict of interest.

Nomenclature

B	Rate of stretching surface	A_1	First Rivlin-Erickson tensor
B^*	Magnetic field strength [NmA^{-1}]	Nu_x	local Nusselt number
C_f	Skin friction coefficient	Sh_x	local Sherwood number
Pr	Prandtl number	τ_w	Shear stress at the wall
M	Magnetic parameter	q_n	heat flux at the wall [Wm^{-2}]
T	Fluid temperature [K]	q_s	wall mass flux
Nbt	Diffusivity parameter	T_w	Surface temperature [K]
Le	Lewis number	T_∞	Ambient temperature [K]
Nc	Heat capacity ratio	U_w	Wall velocity
Sc	Schmidt number	f	Dimensionless stream function
u, v	Velocity components [ms^{-1}]	x, y	Cartesian coordinates
Re_x	local Reynolds number	g	Nanoparticle volume fraction
C	Concentration of nanoparticle	C_w	Concentration of nanoparticle at the surface
C_∞	Ambient concentration of nanoparticle	D_B	Coefficient of Brownian diffusion [$m^{-2}s^{-1}$]
D_T	Coefficient of thermophoresis diffusion [$m^{-2}s^{-1}$]		
Greek Letters			
η	Dimensionless similarity variable	ν	Kinematic viscosity [m^2s^{-1}]
σ	Electrical conductivity [Sm^{-1}]	ρ	Density [kgm^{-3}]
Γ	Positive time constant	λ	Williamson fluid parameter
α	Thermal diffusivity [m^2s^{-1}]	μ	Dynamic viscosity [$kgm^{-1}s^{-1}$]
θ	Dimensionless temperature	ρc	Heat capacity of the fluid [$Jm^{-3}K^{-1}$]
$\rho_p c_p$	Heat capacity of nanoparticles [$Jm^{-3}K^{-1}$]	τ	Extra stress tensor [Nm^{-2}]
Subscripts			
w	Condition at the wall	∞	Condition at the free stream
Superscripts			
'	Derivative w.r.t η		
Abbreviations			
ODEs	ordinary differential equations	PDEs	partial differential equations
MHD	Magnetohydrodynamics		

References

- Williamson, R.V. The flow of pseudoplastic materials. *Ind. Eng. Chem.* **1929**, *21*, 1108–1111. [\[CrossRef\]](#)
- Felder, E.; Levrau, C. Analysis of the lubrication by a pseudoplastic fluid: Application to wire drawing. *Tribol. Int.* **2011**, *44*, 845–849. [\[CrossRef\]](#)
- Cramer, S.D.; Marchello, J.M. Numerical Evaluation of Models Describing Non-Newtonian Behavior. *AIChE J.* **1968**, *14*, 980–983. [\[CrossRef\]](#)
- Lyubimov, D.V.; Perminov, A.V. Motion of a Thin Oblique Layer of a Pseudoplastic Fluid. *J. Eng. Phys. Thermophys.* **2002**, *75*, 920–924. [\[CrossRef\]](#)
- Nadeem, S.; Akbar, N.S. Numerical solutions of peristaltic flow of Williamson fluid with radially varying MHD in an endoscope. *Int. J. Numer. Methods Fluids* **2011**, *66*, 212–220. [\[CrossRef\]](#)
- Akbar, N.S.; Nadeem, S. Carreau fluid model for blood flow through a tapered artery with a stenosis. *Ain. Shams Eng. J.* **2014**, *5*, 1307–1316. [\[CrossRef\]](#)
- Ismail, Z.; Abdullah, I.; Mustapha, N.; Amin, N. A power-law model of blood flow through a tapered overlapping stenosed artery. *Appl. Math. Comput.* **2008**, *195*, 669–680. [\[CrossRef\]](#)
- Ahmed, K.; Akbar, T. Numerical investigation of magnetohydrodynamics Williamson nanofluid flow over an exponentially stretching surface. *Adv. Mech. Eng.* **2021**, *13*, 168781402110198. [\[CrossRef\]](#)
- Ramzan, M.; Liaquet, A.; Kadry, S.; Yu, S.; Nam, Y.; Lu, D. Impact of second-order slip and double stratification coatings on 3D MHD Williamson Nanofluid flow with cattaneo-christov heat flux. *Coatings* **2019**, *9*, 849. [\[CrossRef\]](#)
- Nasrin, R.; Hasanuzzaman, M.; Rahim, N.A. Effect of nano-fluids on heat transfer and cooling system of the photovoltaic/thermal performance. *Int. J. Numer. Methods Heat Fluid Flow.* **2019**, *29*, 1920–1946. [\[CrossRef\]](#)
- Vajravelu, K. Viscous flow over a nonlinearly stretching sheet. *Appl. Math. Comput.* **2001**, *124*, 281–288. [\[CrossRef\]](#)
- Cortell, R. Viscous flow and heat transfer over a nonlinearly stretching sheet. *Appl. Math. Comput.* **2007**, *184*, 864–873. [\[CrossRef\]](#)
- Khan, W.A.; Pop, I. Boundary-layer flow of a nanofluid past a stretching sheet. *Int. J. Heat Mass Transf.* **2010**, *53*, 2477–2483. [\[CrossRef\]](#)
- Van Gorder, R.A.; Sweet, E.; Vajravelu, K. Nano boundary layers over stretching surfaces. *Commun. Nonlinear Sci. Numer. Simul.* **2010**, *15*, 1494–1500. [\[CrossRef\]](#)
- ASHRAE Handbook—Fundamentals SI Edition Atlanta: American Society of Heating; Refrigerating and Air Conditioning Engineers, Inc.: Boca Raton, FL, USA, 2009.
- Kole, M.; Dey, T.K. Viscosity of alumina nanoparticles dispersed in car engine coolant. *Exp. Therm. Fluid Sci.* **2010**, *34*, 677–683. [\[CrossRef\]](#)

17. Dittus, F.W.; Boelter, L.M.K. Heat transfer in automobile radiators of the tubular type. *Int. Commun. Heat Mass Transf.* **1985**, *12*, 3–22. [[CrossRef](#)]
18. Wensel, J.; Wright, B.; Thomas, D.; Douglas, W.; Mannhalter, B.; Cross, W.; Hong, H.; Kellar, J.; Smith, P.; Roy, W. Enhanced thermal conductivity by aggregation in heat transfer nanofluids containing metal oxide nanoparticles and carbon nanotubes. *Appl. Phys. Lett.* **2008**, *92*, 9–12. [[CrossRef](#)]
19. Kulkarni, D.P.; Namburu, P.K.; Ed Bargar, H.; Das, D.K. Convective heat transfer and fluid dynamic characteristics of SiO₂—Ethylene glycol/water nanofluid. *Heat Transf. Eng.* **2008**, *29*, 1027–1035. [[CrossRef](#)]
20. Abdul Hamid, K.; Azmi, W.H.; Mamat, R.; Usri, N.A. Heat transfer performance of titanium oxide in ethylene glycol based nanofluids under transition flow. *Appl. Mech. Mater.* **2014**, *660*, 684–688. [[CrossRef](#)]
21. Li, H.; Xiao, H.G.; Yuan, J.; Ou, J.P. Microstructure of cement mortar with nano-particles. *Compos. Part B Eng.* **2004**, *35*, 185–189. [[CrossRef](#)]
22. Vajjha, R.S.; Das, D.K.; Kulkarni, D.P. Development of new correlations for convective heat transfer and friction factor in turbulent regime for nanofluids. *Int. J. Heat Mass Transf.* **2010**, *53*, 4607–4618. [[CrossRef](#)]
23. Berra, M.; Carassiti, F.; Mangialardi, T. Effects of nanosilica addition on workability and compressive strength of Portland cement pastes Constr. *Build Mater* **2012**, *35*, 666–675. [[CrossRef](#)]
24. Syam Sundar, L.; Venkata Ramana, E.; Singh, M.K.; De Sousa, A.C.M. Viscosity of low volume concentrations of magnetic Fe₃O₄ nanoparticles dispersed in ethylene glycol and water mixture. *Chem. Phys. Lett.* **2012**, *554*, 236–242. [[CrossRef](#)]
25. Azmi, W.H.; Sharma, K.V.; Sarma, P.K.; Mamat, R.; Anuar, S.; Rao, V. Experimental determination of turbulent forced convection heat transfer and friction factor with SiO₂ nano-fluid Exp. *Therm. Fluid Sci.* **2013**, *51*, 103–111. [[CrossRef](#)]
26. Azmi, W.H.; Sharma, K.V.; Sarma, P.K.; Mamat, R.; Anuar, S. Comparison of convective heat transfer coefficient and friction factor of TiO₂ nanofluid flow in a tube with twisted tape inserts. *Int. J. Therm. Sci.* **2014**, *81*, 84–93. [[CrossRef](#)]
27. Namburu, P.K.; Kulkarni, D.P.; Misra, D.; Das, D.K. Viscosity of copper oxide nanoparticles dispersed in ethylene glycol and water mixture. *Exp. Therm. Fluid Sci.* **2007**, *32*, 397–402. [[CrossRef](#)]
28. Nguyen, C.T.; Desgranges, F.; Roy, G.; Galanis, N.; Maré, T.; Boucher, S.; Angue Mintsa, H. Temperature and particle-size dependent viscosity data for water-based nanofluids—Hysteresis phenomenon. *Int. J. Heat Fluid Flow.* **2007**, *28*, 1492–1506. [[CrossRef](#)]
29. Jang, S.; Choi, S.U.S. Effects of Various Parameters on Nanofluid Thermal Conductivity. *J. Heat Transf.* **2007**, *129*, 617–623. [[CrossRef](#)]
30. Prasher, R.; Bhattacharya, P.; Phelan, P.E. Thermal conductivity of nanoscale colloidal solutions (nanofluids). *Phys. Rev. Lett.* **2005**, *94*, 3–6. [[CrossRef](#)]
31. Awan, A.U.; Abid, S.; Ullah, N.; Nadeem, S. Magneto hydrodynamic oblique stagnation point flow of second grade fluid over an oscillatory stretching surface. *Results Phys.* **2020**, *18*, 103233. [[CrossRef](#)]
32. Abel, M.S.; Mahesha, N. Heat transfer in MHD viscoelastic fluid flow over a stretching sheet with variable thermal conductivity, non-uniform heat source and radiation. *Appl. Math. Model.* **2008**, *32*, 1965–1983. [[CrossRef](#)]
33. Sreedevi, P.; Sudarsana Reddy, P.; Chamkha, A.J. Heat and mass transfer analysis of nanofluid over linear and non-linear stretching surfaces with thermal radiation and chemical reaction. *Powder Technol.* **2017**, *315*, 194–204. [[CrossRef](#)]
34. Jahan, S.; Sakidin, H.; Nazar, R.; Pop, I. Flow and heat transfer past a permeable nonlinearly stretching/shrinking sheet in a nano-fluid: A revised model with stability analysis. *J. Mol. Liq.* **2017**, *233*, 211–221. [[CrossRef](#)]
35. Sakiadis, B.C. Boundary—Layer behavior on continuous solid surfaces: III. The boundary layer on a continuous cylindrical surface. *AIChE J.* **1961**, *7*, 467–472. [[CrossRef](#)]
36. Sakiadis, B.C. Boundary—Layer behavior on continuous solid surfaces: II. The boundary layer on a continuous flat surface. *AIChE J.* **1961**, *7*, 221–225. [[CrossRef](#)]
37. Sakiadis, B.C. Boundary—Layer behavior on continuous solid surfaces: I. Boundary—layer equations for two—dimensional and axisymmetric flow. *AIChE J.* **1961**, *7*, 26–28. [[CrossRef](#)]
38. Crane, L.J. Flow past a stretching plate. *Z. Angew. Math. Phys. ZAMP* **1970**, *21*, 645–647. [[CrossRef](#)]
39. Gupta, P.S.; Gupta, A.S. Heat and Mass Transfer on a Stretching Sheet. *Can. J. Chem. Eng.* **1977**, *55*, 744–746. [[CrossRef](#)]
40. Kameswaran, P.K.; Narayana, M.; Sibanda, P.; Murthy, P.V.S.N. Hydromagnetic nanofluid flow due to a stretching or shrinking sheet with viscous dissipation and chemical reaction effects. *Int. J. Heat Mass Transf.* **2012**, *55*, 7587–7595. [[CrossRef](#)]
41. Khan, U.; Ahmad, S.; Hayyat, A.; Khan, I.; Nisar, K.S.; Baleanu, D. On the Cattaneo-Christov heat flux model and OHAM analysis for three different types of nanofluids. *Appl. Sci.* **2020**, *10*, 886. [[CrossRef](#)]
42. Rashidi, M.M.; Keimanesh, M.; Hung, T.K. Magneto hydrodynamic Biorheological transport phenomena in a porous medium: A simulation of magnetic blood flow control and filtration. *Int. J. Numer. Method Biomed. Eng.* **2011**, *27*, 805–821. [[CrossRef](#)]
43. Oughton, S.; Matthaeus, W.H.; Dmitruk, P. Reduced MHD in Astrophysical Applications: Two-dimensional or Three-dimensional. *Astrophys. J.* **2017**, *839*, 2. [[CrossRef](#)]
44. Carle, F.; Bai, K.; Casara, J.; Vanderlick, K.; Brown, E. Development of magnetic liquid metal suspensions for magneto hydrodynamics. *Phys. Rev. Fluids* **2017**, *2*, 1–20. [[CrossRef](#)]
45. Pedchenko, A.; Gelfgat, Y. Study of the influence of current frequency and non-magnetic gap value on the efficiency of al-alloys stirring in metallurgical furnaces. *Magneto hydrodynamics* **2007**, *43*, 363–375. [[CrossRef](#)]

46. Hainke, M.; Friedrich, J.; Vizman, D.; Müller, G. MHD effects in semiconductor crystal growth and alloy solidification. In Proceedings of the International Scientific Colloquium, Modelling for Electromagnetic Processing, Hannover, Germany, 24–26 March 2003; pp. 73–78.
47. Hussain, Z.; Hayat, T.; Alsaedi, A.; Ullah, I. On MHD convective flow of Williamson fluid with homogeneous-heterogeneous reactions: A comparative study of sheet and cylinder. *Int. Commun. Heat Mass Transf.* **2021**, *120*, 105060. [[CrossRef](#)]
48. Nadeem, S.; Hussain, S.T. Flow and heat transfer analysis of williamson nanofluid. *Appl. Nanosci.* **2014**, *4*, 1005–1012. [[CrossRef](#)]
49. Nadeem, S.; Hussain, S.T.; Lee, C. Flow of a williamson fluid over a stretching sheet. *Braz. J. Chem. Eng.* **2013**, *30*, 619–625. [[CrossRef](#)]